Exposed and Transcutaneous Measurement of Musculoskeletal Tissues using Fiber Optic Coupled Raman Spectroscopy

Francis W.L. Esmonde-White[a], Karen A. Esmonde-White[b], Michael D. Morris[*a]

[a] University of Michigan, Department of Chemistry, Ann Arbor, MI 48109-1055;
[b] University of Michigan Medical School, Department of Internal Medicine, Ann Arbor, MI 48109

ABSTRACT

Raman spectroscopic measurement of bone composition has shown promise as a medical diagnostic by measuring the molecular composition of the bone mineral and matrix. We previously demonstrated proof-of-principle transcutaneous Raman spectroscopy bone measurements in human cadavers. In this paper, we discuss further optimization of the instrumental configuration for efficient collection of bone signal using contact fiber-optic probe designs. To optimize collection of Raman signal through overlaying soft tissue, novel geometrically-accurate tissue phantoms were prepared. MRI and CT images of the human cadaveric specimens were used to create solid tissue phantoms with accurate geometric dimensions. In these tissue phantoms, optical properties can be varied systematically. Raman spectra of the prepared tissue phantoms were used to optimize the positions of the fibers in the fiber optic system, and the laser illumination sequence in the measurements. Three fiber optic probes were developed and tested with both novel tissue phantoms and human cadaveric specimens. The contact fiber optic probes were developed for arthroscopic measurements of joints, for transcutaneous measurements of bone in situ, and for contact measurements of exposed bone. By coupling the fiber optic probe to an imaging spectrograph, spectra were collected simultaneously at many positions on the tissue. Furthermore, spectra were collected with several different excitation laser patterns to enhance the effective spatial resolution of the measurements. Finally, a series of improvements were made in the data preprocessing to improve the recovered spectral signal. Together, these modifications improve signal-to-noise and spatial resolution.

Keywords: Raman spectroscopy, Raman tomography, biomedical diagnosis, geometrically and optically accurate tissue phantom, fiber optic Raman probe, transcutaneous, osteoporosis

1. INTRODUCTION

The use of Raman microspectroscopy to identify damaged or diseased tissue has been well-established.[1] Raman spectra are rich with spectral features that include well-defined bands, and so a single spectrum can not only identify chemical composition but also provide insight into molecular structure such as protein secondary structure, bone mineral crystallinity or biopolymer entanglement. Spectral features are correlated to progression of many types of cancer and other illnesses.[2-6] Fiber optic probes for biomedical Raman spectroscopy have received much attention in the past 10 years because it enables measurement of equivalent spectral features, but in a non-invasive manner.

Transcutaneous Raman spectroscopy and tomography of bone tissue have been demonstrated using fiber-optic probes where the illumination and collection fibers are spatially offset.[7-11] Bone Raman signal has been recovered through 1-4 cm of overlaying soft tissue in transmission geometries. These earliest studies alluded to the potential for TRS as a clinical tool for diagnosis of bone related diseases. Similar to other applications for *in vivo* Raman spectroscopy, a significant challenge is in the development of appropriate fiber optic probes.[12, 13] Technological challenges of probe development include: determining an appropriate excitation wavelength and intensity, optimizing spatial resolution, and reducing the effect of tissue autofluorescence on the collection of Raman spectra. Important safety considerations center on laser fluence at the skin, and potential ocular exposure for both the patient and instrument operator. In this regard, standards of acceptable limits of laser fluence or laser exposure have been established by government agencies for skin and eye tissues.

In this paper, we report the use of small, custom designed fiber optic probes for the purpose of collecting Raman spectra from musculoskeletal tissues. Tissue phantoms were developed and used to test various geometric tissue models with optical probes. Transcutaneous Raman studies in cadaveric human tissue were performed to measure the capability of three custom designed probes to collect Raman spectra of bone. During these experiments, we monitored the skin for any potential laser-induced tissue damage. Two sets of needle-like fiber optic probes with different fiber-optic diameters

enabled manipulation of source-detector separation and sampling geometry. A pen-like fiber optic probe was designed to encompass a range of source-detector separations and was used to examine exposed tissues. Measurements of directly exposed tissues using the pen-probe served to validate transcutaneous bone measurements. Additionally, the pen-probe was used as a prototype for Raman arthroscopy that examined exposed articular cartilage in joint spaces.

2. METHODOLOGY

Raman spectroscopy instrumentation

Three custom-designed fiber optic probes were constructed for tissue measurements (FiberTech Optica Inc., Kitchener ON, Canada). The first probe (called the 4mm probe) consisted of 15 200 μm core diameter illumination fibers and 50 100 μm core diameter collection fibers. Collection fibers were bundled into ten groups of 5 fibers, with each group contained in an independent stainless steel ferrule. The outer diameter of the ferrule was 1.25 mm at the tip and 4 mm at the base. The second probe (called the fine fiber probe) consisted of 19 200 μm core diameter illumination fibers and 50 100 μm core diameter collection fibers. The 50 collection fibers were encased individually in 50 separate branches. Each branch was terminated in a 220 μm outer diameter stainless steel ferrule. The third probe (called the pen-probe) consisted of 19 200 μm core diameter illumination fibers and 50 100 μm core diameter collection fibers. The fibers were arranged into a disc and ring, with collection fibers in both the disc and ring, and illumination fibers in the outer ring only. All three fiber optic probes had illumination and collection fibers 3 meter in length. For each probe, the collection fiber bundles were attached to the Raman spectrometer using PhAT probe fiber connector assemblies (RXN-FCA-PhAT, Kaiser Optical Systems Inc., Ann Arbor, MI) allowing the fiber optic probes to be easily switched without realignment of the instrument. An axial-transmissive Raman spectrograph equipped with an 830 nm excitation laser and optimized for collection of near-infrared signal was used throughout the studies (RamanRxn1, Kaiser Optical Systems Inc.). Laser light was coupled through a 100 μm core diameter fiber and then focused into the illumination fiber bundle. Two 830 nm Raman lasers were used with the transcutaneous measurements. The first laser had a 400 mW output prior to the fiber optic coupling (Invictus, Kaiser Optical Systems Inc.). The second laser provided 600 mW at the output of the coupled fiber optic (Innovative Photonics Solutions, Monmouth Junction, NJ).

Raman spectroscopy of human cadaveric limbs

Cadaveric human upper and lower extremities were examined with the three fiber optic probes. In each case, transcutaneous measurements were acquired prior to dissection of the specimen to acquire spectra of various isolated and exposed tissues (including cortical bone, cancellous bone, cartilage, muscle, fat, tendon and skin). Cadaveric human upper and lower extremities were acquired from the University of Michigan Medical School Anatomical Donations program. Prior to the transcutaneous measurements, glycerol was topically applied as an optical clearing agent and allowed to soak for 20 minutes. A fresh layer of glycerol was then again applied and the limb was covered with a thin sheet of plastic wrap to limit potential contamination of the probe. After collection of the transcutaneous measurements, the overlaying soft tissue and periosteum were removed to expose the bone of the distal radius or of the proximal tibia. Raman spectra of the exposed cortical bone were collected using the pen-like fiber optic probe. A small section (2 cm) of cortical bone was removed using a surgical saw, and Raman spectra were collected of the exposed cancellous bone using the pen-probe.

As a reference, spectra were collected for some of the tissue specimens with a 785 nm Raman microscope. A line-focused Invictus laser (Kaiser Optical Systems) operating at 785 nm (~ 80 mW) was used to illuminate specimens on an upright Nikon E600 epi-illumination microscope (Nikon, Melville, NY). Raman scatter was dispersed through an axial transmissive spectrometer (HoloSpec ƒ1.8, Kaiser Optical Systems). Raman signal was collected for 1-10 minutes on a 1024x128 back-illuminated deep depletion CCD camera (Andor Technology, Belfast, UK).

Calibration spectra from a neon emission source and a NIST-traceable white light source were collected on the Raman spectrograph using the Kaiser HoloSpec Calibration Accessory (HCA, Kaiser Optical Systems Inc., Ann Arbor, MI). Spectra of teflon and cyclohexane were collected for calibration and validation of the laser wavelength. For each spectral measurement, 10 image frames were acquired. Each frame was collected over a 60 second integration interval.

Data preprocessing

Raman images, consisting of 256x1024 pixels, were collected using the Andor Solis software, exported as ASCII format, then imported into Matlab (The MathWorks, Natick, MA) for preprocessing using software routines written in-house.[14]

For each Raman image, 10 image frames were collected. The image stack was first combined to correct for cosmic rays.[15] A mean image from the 10 replicate image frames was calculated after removing all outlier pixel intensities more than 5 standard deviations from the median image (each x-y pixel position was treated independently). Images were then corrected for optical distortions in the dispersion axis. The recorded Raman image was transformed using a technique adapted from the field of remote sensing. In remote sensing, image registration is used to align images taken from different perspectives.[16, 17] A polynomial field curvature correction was applied to remove imperfections in the camera rotation, as well as dispersion nonlinearities and slit-image curvature. The field curvature was corrected so that the dispersion (wavelength) axis was horizontal to the image axis, while the spatial (slit position) axis was vertical to the image axis. Control points consisted of measured (imperfect) and ideal positions which were used to define the field curvature as a third order polynomial. Image registration also corrected for slight rotational misalignment in the CCD orientation. Once the image field was corrected, intensities detected at each fiber were determined using a least squares fitting of measured white calibration images. White-light images were individually collected from all collection fibers, and intensity profiles of each collection fiber were determined using a least-square fitting of the measured white-light image. Silica contributions to the measured spectra are significant with the long and unfiltered fiber-optics employed here. Silica contributions were measured by reflecting the excitation laser from a roughened aluminum surface, and removed from the measured data using a derivative subtraction of the measured silica spectra.[18]

Preparation of Tissue Phantoms

The procedure for preparation of tissue phantoms for Raman spectroscopy will be described in a paper currently in preparation. Briefly, three dimensional geometrically-accurate gelatin tissue phantoms were reproduced from CT scans of human upper and lower extremities. Prior to CT scanning, the limbs were thawed in a 4°C refrigerator overnight. Limbs were kept in a plastic bag during CT scans to prevent contamination of the clinical high-resolution computed tomography instrument. CT images were collected in the sagittal, coronal and transverse planes using a high-resolution 64 slice clinical CT instrument (Siemens Somatom Sensation Cardiac 64, Siemens Healthcare, Germany). Each slice consisted of a 250 mm field of view, slice thickness 0.6 mm, pitch 0.55. Three dimensional CT reconstructions were transformed into 2D surface meshes using Mimics software (Materialise, Leuven, Belgium). Mimics renderings of a knee and wrist were transferred to 3D Studio Max (Autodesk Inc., San Rafael, CA) to produce images and generate video models. Three dimensional plaster models were printed using a Spectrum Z510 rapid prototype instrument (Z Corporation, Burlington, MA). A multi-step molding process using urethane and silicone room temperature vulcanizing rubber was used to create gelatin 3D models from the plaster prints. The gelatin phantoms were cast into the silicone rubber molds in a multistep casting process. Examples of the resulting tissue phantoms are shown in Figure 1. Raman spectra of the tissue phantoms were collected using the pen-probe.

3. RESULTS AND DISCUSSION

Effective measurement of transcutaneous Raman bone spectra is limited by the optical probes used to collect spectra. To improve transcutaneous Raman spectra, the collected elastically scattered excitation laser light must be minimized (which helps to reduce the fluorescence background), while maximizing the collection of Raman-shifted light. Geometry and optical properties both influence optical sampling, and so we have developed geometrically accurate tissue phantoms with tissue-relevant chemical composition and optical properties for optimizing optical probes. Using these phantoms we tested various fiber optic probe configurations for specific anatomical sampling locations. The influence of geometry on
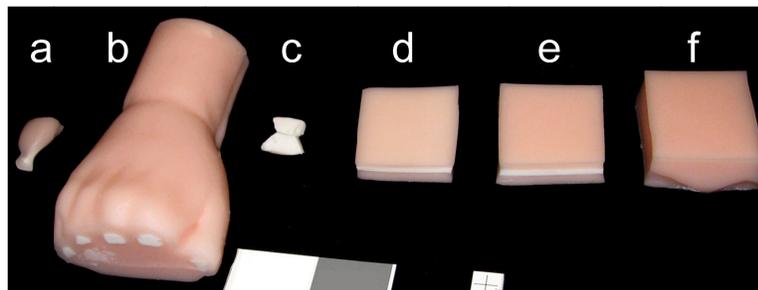
Figure 1. Gelatin tissue phantoms in variety of geometries. At left are two geometrically-accurate tissue phantoms, with a) showing a rat tibia model, and b) showing a human distal radius model. At right are four planar tissue phantoms, with c) showing a block of hydroxyapatite in gelatin as a bone layer, d) thin planar phantom, e) thick planar phantom, and f) layer simulating soft tissue.

the recovered spectrum is substantial, as shown in Figure 2, where the sampling position clearly influences the relative intensity of the phosphate ν_1 (960 cm^{-1}) band to the fluorescence background. All spectra shown in Figure 2 were acquired with the pen-probe with a fixed source-detector pattern.
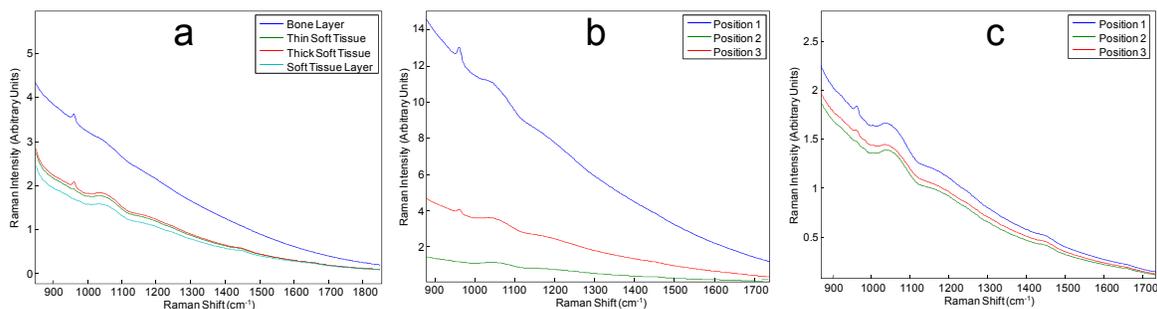
Figure 2. Raman spectra of tissue phantoms with a) planar geometry, b) rat tibia geometry, and c) human distal radius geometry. An intense fluorescence was present in the bone layer, the bone layer spectrum intensity was divided by 10 to bring it onto the same scale as the other spectra.

Transcutaneous measurements were collected of the distal radius using the 4mm fiber optic probe. Spectra were measured for several different patterns of collection and illumination fibers as shown in Figure 3. A fiber-optic probe holder allowed easy exchange of the fiber positions. The fiber-optic probe holder was placed on the wrist of a cadaveric human upper extremity. As expected, a higher bone Raman signal was recovered using patterns with a greater source-detector separation (Patterns 1-5). Using these patterns, bands attributed to bone mineral (phosphate $\nu_1 \sim 960$ cm^{-1}) and collagen protein (ring breathing mode ~ 1002 cm^{-1}) become more visible. For patterns that illuminate fibers close to collection fibers, the resulting spectra (Patterns 6 & 7) are dominated by soft tissue lipid bands with minor contributions from the bone mineral.
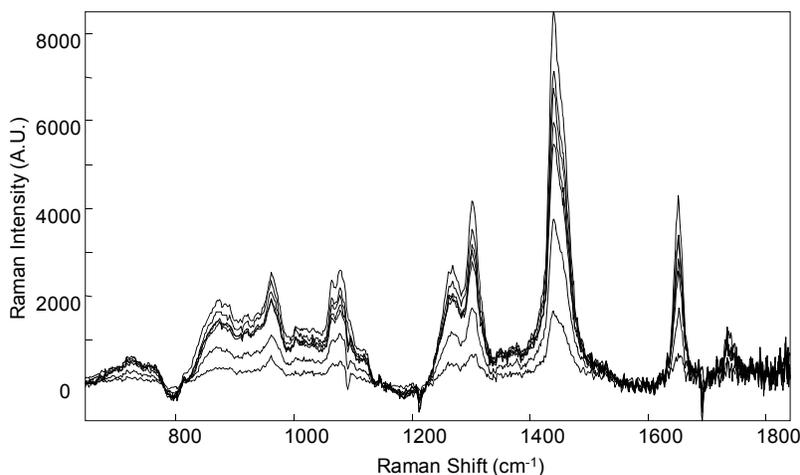
Figure 3. Transcutaneous Raman spectra of human distal radius collected with different illumination/collection patterns using the 4mm fiber optic probe. The intensity of the phosphate ν_1 band at 960 cm^{-1} varied with source-detector separation. Bands arising from soft tissue lipids are evident in all spectra.

The first tests using the 4mm fiber optic probe demonstrated a proof-of-principle that a fiber probe consisting of individual illumination and collection fibers could be used to recover transcutaneous Raman bone signal. A second generation probe was developed so that the 50 collection fibers, encased individually, could be positioned with better contact on skin. Transcutaneous Raman bone signal recovered from the fine fiber probe, shown in Figure 4, has similar spectral features to other transcutaneous Raman measurements. These results show that the dominant spectral features of the transcutaneous Raman spectrum in Figure 4a arise from soft tissue lipids. The bone phosphate band at ~ 960 cm^{-1} is visible in transcutaneous measurements. After transcutaneous measurements were completed, soft tissue and the periosteum were dissected, exposing the cortical bone. A small segment of bone was removed using a surgical saw,

exposing trabecular bone. Exposed cortical (solid line) and trabecular (dashed line) bone spectra were collected using the pen-probe, shown in Figure 4b. Measurements of cortical using the pen-probe had similar spectral features as spectra obtained on a 785 nm Raman microscope, indicating that the pen-probe is a good tool for exposed bone measurements (data not shown). As expected, exposed bone spectra revealed differences primarily in the 1200-1700 cm^{-1} region corresponding to the organic matrix of bone. In cortical bone, this region contains contributions from the collagen matrix, while in trabecular bone the bands are assigned to marrow lipids. Lipid bands in spectra from trabecular bone at ~1300 cm^{-1}, 1435 cm^{-1}, 1655 cm^{-1} and 1725 cm^{-1}, are similar to lipid bands observed in transcutaneous measurements.
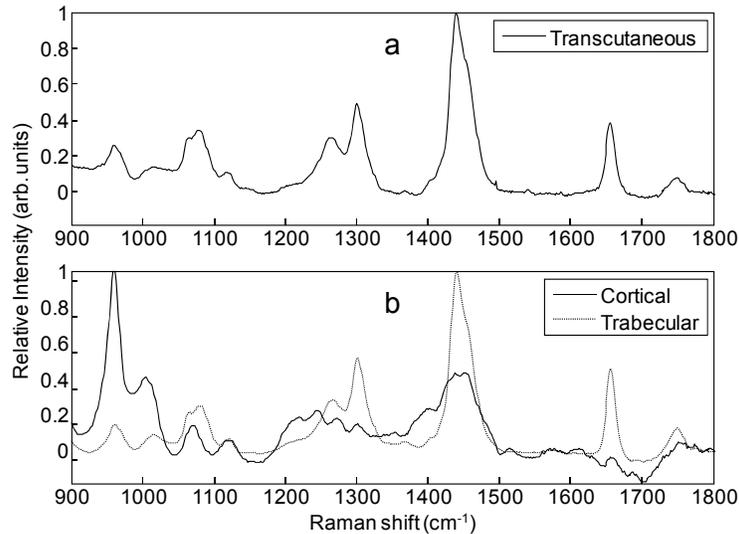
Figure 4. Raman spectra of human proximal tibia measured a) transcutaneously using the needle-like probe and b) exposed cortical (solid line) and trabecular (dashed line) bone using the pen-probe.

4. CONCLUSIONS

Transcutaneous Raman spectroscopy and imaging of bone tissue has potential as a clinical tool to non-invasively assess alterations in bone chemistry associated with bone disease or infection. In this paper, we present practical approaches toward validating and testing next generation contact probes for transcutaneous Raman spectroscopy. Gelatin tissue phantoms with accurate physiological geometries were created from CT scans of human arm and leg extremities. Tissue phantoms were used for several purposes including: to test illumination/collection geometries, systemically control the chemical properties of the bone and soft tissue layer, and study the effects of tissue geometry on recovery of subsurface Raman signal.

Our first generation of non-contact probes used probe geometries where collection fiber optics were spatially offset from illumination fiber optics, enabling recovery of bone Raman signal underlying 1-4 cm of soft tissue. The first studies further demonstrated that recovery of bone signal is possible not only for single-point Raman spectroscopy but also for 3D Raman tomographic imaging. In this study, two contact probes were designed and tested on human cadaveric tissue. The contact probes improved spatial resolution and enabled a wider variety of illumination/collection geometries. Transcutaneous Raman signal of bone was recovered using both the 4mm and fine fiber probes. The intensity of the bone signal was dependent upon the illumination/collection pattern and the specimen geometry, as expected. Reference measurements on exposed cortical and trabecular bone were collected using the pen-probe. These preliminary results show that bone signal can be recovered from 1-3 cm of overlying soft tissue using contact probes. Further examination of the transcutaneously measured data using principle components analysis, self-modeling curve resolution, and tomographic spatial reconstructions should improve the recovery of bone Raman bands, resolve bone collagen matrix bands and the carbonate band at ~ 1070 cm^{-1}, and enable transcutaneous measurements of trabecular bone tissue.

5. ACKNOWLEDGEMENTS

6. REFERENCES

[1] H.-U. Gremlich and B.Yan, Eds, [Infrared and Raman Spectroscopy of Biological Materials], Marcel Dekker Inc, New York, (2001).

[2] Ermakov, I. V., Ermakov, M. R., Gellermann, W., and Bernstein, P. S., "Macular pigment Raman detector for clinical applications", J.Biomed. Opt. 1(9), 139 (2004).

[3] Motz, J. T., Gandhi, S. J., Scepanovic, O. R., Haka, A. S., Kramer, J. R., Dasari, R. R., and Feld, M. S., "Real-time Raman system for in vivo disease diagnosis", J.Biomed. Opt. 3(10), 031113 (2005).

[4] Krafft, C., Sobottka, S. B., Schackert, G., and Salzer, R., "Raman and infrared spectroscopic mapping of human primary intracranial tumors: a comparative study", J. Raman Spectrosc. 1-3(37), 367 (2006).

[5] Filik, J. and Stone, N., "Analysis of human tear fluid by Raman spectroscopy", Anal. Chim. Acta 2(616), 177 (2008).

[6] Esmonde-White, K. A., Mandair, G. S., Raaii, F., Jacobson, J. A., Miller, B. S., Urquhart, A. G., Roessler, B. J., and Morris, M. D., "Raman Spectroscopy of Synovial Fluid as a Tool for Diagnosing Osteoarthritis", J. Biomed. Opt. 3(14), 034013 (2009).

[7] Schulmerich, M. V., Dooley, K. A., Morris, M. D., Vanasse, T. M., and Goldstein, S. A., "Transcutaneous fiber optic Raman spectroscopy of bone using annular illumination and a circular array of collection fibers", J. Biomed. Opt. 11(6), 060502 (2006).

[8] Matousek, P., "Inverse Spatially Offset Raman Spectroscopy for Deep Noninvasive Probing of Turbid Media", Appl. Spectrosc. 60(11), 1341 (2006).

[9] Schulmerich, M. V., Cole, J. H., Dooley, K. A., Kreider, J. M., Goldstein, S. A., and Morris, M. D., "Optical clearing in transcutaneous Raman spectroscopy of murine cortical bone tissue", J. Biomed. Opt. 2(13), 021108 (2008).

[10] Schulmerich, M. V., Cole, J. H., Dooley, K. A., Morris, M. D., Kreider, J. M., Goldstein, S. A., Srinivasan, S., and Pogue, B. W., "Noninvasive Raman tomographic imaging of canine bone tissue", J.Biomed. Opt. 2(13), 020506 (2008).

[11] Srinivasan, S., Schulmerich, M., Cole, J. H., Dooley, K. A., Kreider, J. M., Pogue, B. W., Morris, M. D., and Goldstein, S. A., "Image-guided Raman spectroscopic recovery of canine cortical bone contrast in situ", Opt. Express 16(16), 12190 (2008).

[12] I. R. Lewis and H. G. M. Edwards, Eds, [Handbook of Raman Spectroscopy: From the Research Laboratory to the Process Line], Marcel Dekker, New York, (2001).

[13] T. Vo-Dinh, Ed. [Biomedical Photonics Handbook], CRC Press, Boca Raton, (2003).

[14] Esmonde-White, F. W. L., Schulmerich, M. V., Esmonde-White, K. A., and Morris, M. D., "Automated Raman spectral preprocessing of bone and other musculoskeletal tissues", Proc. SPIE 7166, 716605 (2009).

[15] Horne, K., "An Optimal Extraction Algorithm for CCD Spectroscopy", Publ. Astron. Soc. Pac. 98, 609-617 (1986).

[16] Richards, J. A. and Jia, X., [Remote Sensing Digital Image Analysis] Springer-Verlag, Berlin, Germany, 3rd ed, (1999).

[17] Schowengerdt, R. A., [Remote Sensing] Academic Press, San Diego, CA, 2nd ed, (1997).

[18] Banerjee, S. and Li, D., "Interpreting Multicomponent Infrared Spectra by Derivative Minimization", Appl. Spectrosc. 6(45), 1047 (1991).